Preparation, microstructural and optical Characterization of NiO nanoparticles

M. A. Kaid
[1]*Physics Department, Faculty of Science, El-Minia University, El-Minia, Egypt*

Abstract

A fine NiO powders were prepared by a homogeneous precipitation method with an aqueous solution of nickel nitrate hexahydrate and citric acid. The microstructure, surface morphology of NiO were characterized by thermo gravimetric (TGA) analysis and differential scanning calorimeter (DSC) , X-ray diffraction (XRD), scanning electron microscope (SEM) , infrared (IR) spectroscopy. The experiment results show that the NiO nanoparticles are cubic structure with spherical shape and well dispersed, the particle size distribution ranging from 7 to 28 nm with the average particle size is about 15.5 nm. The infrared absorption band of NiO nanoparticles shows blue shifts compared with that of bulk NiO. The optical band gap energy value 3.81 eV has been determined from absorbance spectra in strong absorption region.

Keywords: Nanoparticle NiO; XRD; SEM; Crystallite size; Energy gap.

1-Introduction

In recent years, nanomaterials have received growing interests as a result of their peculiar and fascinating properties and applications superior to their bulk counterparts. Nanomaterials have been widely used in various fields, such as photoelectric, recording materials, catalysts, sensors, ceramic materials, etc., due to

their special structures and properties [1, 2]. A fine nickel oxides are very promising functional materials [3]. They have been widely used in the product ion of battery electrodes, catalysts, semiconductor materials (such as piezoresistors, thermistors), the gas sensor materials [4], nickel zinc ferrite [5], stain glass, ceramic additives [6]. Nanostructures nickel and its oxides are of special interest because of their electronic and magnetic properties and their surface chemistry [7, 8]. NiO is a stable wide direct band-gap material (3.56 eV) and exhibits p-type semiconducting behavior [9]. Nanosized NiO can be superparamagnetic and superanti-ferromagnetic [10]. Such nanostructures have potential applications in catalysis, rechargeable batteries, and fuel cells [11]. Thus the ability to generate such minuscule structures is essential to much of modern science and technology [12–16]. Techniques for the nano-scale particle preparation have been developed in the last years and can be divided into three major classes: chemical, mechano-chemical and thermophysical methods [17, 18]. In the present work, NiO phase was prepared using $Ni(NO_3)_2 \cdot 6H_2O$ and citric acid as the reduction agent by the sol-gel self propagating, low temperature combustion process. The morphology of the NiO was measured using a scan electron microscope (SEM) and X-ray diffractgram. The optical properties of NiO have been determined via absorbance spectrum and the optical band gap has been determined.

2- Experimental

Certain amount of $Ni(NO_3)_2 \cdot 6H_2O$ was dissolved in distilled water, then 2 mol of citric acid was added for each mol of metal ion and the mixture was heated at 90 °C for 2 h. Then the solution was moved to cold water, quenched for 20 min and filtrated, washed with deionized water and alcohol three times respectively and dried at 110 °C for 2 h to obtain the precursor. The precursor was calcinated at 300~ 450 °C

(according to TGA/DSC curve that mentioned below) for 4 h to get superfine NiO powders. The thermal behavior of the precursor was analyzed by thermogravimetric analysis (TGA) and differential scanning calorimetry (DSC) (Shimadzu 50 with an accuracy of ±0.1 K). The value of the glass transition, T_g, the crystallization extrapolated onset, T_{in} and the crystallization peak, T_p, temperature were determined with accuracy ±1 K by using the microprocessor of the thermal analyzer. The structure and phases of the powder sample was identified by means of X-ray powder diffraction (XRD) Shimadzu Diffractometer XRD 6000, Japan, with Cu-Kα_1 radiation (λ = 1.54056 Å). The data was collected by step-scan modes in a θ-2θ range between 4° and 80° with step-size of 0.02° and step time of 0.6 seconds. Pure Silicon ~ Si 99.9999 % was used as an internal standard. The surface morphology of nanoparticles was observed by means of a scanning electron microscope SEM (JOEL XL) operating at an accelerating voltage of 30 kV. The relative error of determining the indicated elements does not exceed 2 %. The IR absorption spectra of the glasses in the wave number range of 400–2000 cm^{-1} with a resolution of 4 cm^{-1} were recorded at room temperature by an IR spectrophotometer type JASCO, FT/IR-430 (Japan), using the KBr pellet technique. Optical characterization of the powder sample on transparent plaster has been preformed from spectral absorbance, which was obtained through JASCO V-670 double beam spectrophotometer. The measurements have been performed in the wavelength range from 200 to 2500 nm. The optical properties of NiO have been determined via absorbance spectrum and the optical band gap was determined

3- **Results and Discussion**

Fig . 1 shows thermal curves of the precursor. From the TG curve, it can be seen that except for the weight loss before 200 ^{o}C, which is due to loss of physical absorbed water on the surface of the precursor. Most of the weight loss of the precursor takes place between 300 ^{o}C and 360 ^{o}C, which is caused by the thermal decomposition of the precursor above 400 ^{o}C, there is no weight loss at T_G curve, indicating that the decomposition is complete. Accordingly, a strong exothermic peak on DSC curve appears between 335 ^{o}C and 365 ^{o}C.

Fig. 1(a) shows the DSC traces for of the precursor at heating rate 10 K/min, this figure displays a crystallization peak, which consists of two overlapped crystallized peaks. Fig. 2 shows the separation of two overlapped crystallized peaks. The indices 1 and 2 in T_{p1} and T_{p2} denote to the first peak and the second peak, respectively. The presence of two peaks means that there are two phases appear during the crystallization process. The phases at which the alloy crystallizes after the thermal process have been identified by X-ray diffraction.

To identify the possible phases that crystallizes during the thermal treatment applied to the samples, the X-ray diffraction patterns of the precursor annealed at 200, 335, 350 and 365 ^{o}C, each one for 2 h. Fig. 3a shows the most relevant portions of the diffractgram for the precursor at 200 ^{o}C, which show characteristics of the amorphous phase of the precursor at diffraction angles (2θ) between 4^{o} and 70^{o}. To identify the possible phases that crystallizes according to TGA and DSC curves shown in Fig. 1. The X-ray diffraction patterns of the precursor annealed at the first peak of crystallization temperature (T = 335 ^{o}C) with a heating rate of 10 ^{o}C /min for 2 h. Fig 3b represents the diffractogram of the transformed material after the crystallization process suggests the presence of nanocrystallites of two phases, the first is Ni according to JCPDS 1-1258, which crystallizes in the cubic structure at 2θ = 44.241^{o}

and 51.602^{o} corresponding to C(111) and C(200) orientations with lattice parameters a = b = c = 0.354 nm and the second is NiO according to JCPDS 2-1216, which crystallites in the cubic structure at 2θ = 37.009^{o}, 43.165^{o} and 62.672^{o} corresponding to C(111), C(200) and C(220) orientations with lattice parameters a = b = c = 0.417 nm. Fig. 3c shows the X-ray diffraction patterns of the precursor annealed at 350 ^{o}C with heating rate of 10 ^{o}C /min for 2 h. The crystallization process in Fig. 3c suggests the presence of a major of nanocrystallites of NiO phase and small traces of Ni phase. When the annealing temperature increase to second peak of crystallization temperature (T = 365 ^{o}C that appear in Fig. 2) with a heating rate of 10 ^{o}C /min for 2 h, only NiO phase appear as shown in Fig. 3d according to the mentioned above JCPDS card.

The XRD pattern shows a significant amount of line broadening which is a characteristic of nanoparticles. The crystal size for both Ni and NiO peaks at different temperature of annealing can be calculated according to Debye-Scherrer formula [19].

$$D = \frac{k\lambda}{\beta \cos\theta} \quad (1)$$

Where k=0.9, λ is the wavelength of the Cu-Kα radiations, β is the full width at half maximum and θ is the angle obtained from 2θ values corresponding to maximum intensity peak in XRD pattern. The calculated crystallite size value of each peaks are listed in table 1. It is observed that the crystallite size decreases with increasing the annealing temperature. The decrease in crystallite size may attribute to the increase in the FWHM at each reflection with increasing the annealing temperature [20]. Such an increase in FWHM may be owing to the decreasing in lattice defects among the grain boundary. Bragg's law was used to calculate inter planar space [21].

$$n\lambda = 2d\sin(\theta) \quad (2)$$

Where *n* was taken as 1. The values of *d* for the intense peak are listed in table 1. The diffraction peaks thus obtained from X-ray diffraction data are in good agreement with the standard patterns for Ni and NiO.

Fig. 4 shows the SEM image of NiO nanoparticles at annealing temperature 365^{o}C with magnification of 70000 X. From the data obtained by SEM micrographs, the particle size histograms can be drawn and the mean size of the particles can be determined using SEM with developed software (Image Processing and Analysis in Java) [22]. Figure 5 shows the particle size distribution of NiO nanoparticles. It can be seen that the particle sizes possess a small and narrow size distribution in a range from 7 to 28 nm, and the mean diameter (taken as average particle diameter) is about 15.5 nm. The mean particle size determined by SEM is in good agreement with the average crystallite size calculated by the Scherer formula from the XRD patterns [23]. However, at this magnification, it is clear to see that many nanoparticles are absorbed on the surface of large particles to form aggregates. This is because those small particles have big surface area, high surface free energy, and unstable structure, and can gather easily to form big aggregates in order to reduce their surface energy. Figure 6 shows the IR spectra of NiO nanoparticles, which showed several significant absorption peaks. The broad absorption band in the region of 600–700 cm^{-1} is assigned to Ni–O stretching vibration mode; the broadness of the absorption band indicates that the NiO powders are nanocrystals. The size of samples used in this study was much less than the bulks form NiO, so that NiO nanoparticles had its IR peak of Ni–O stretching vibration and shifted to blue spectrum. Due to their quantum size effect and spherical nanostructures, the IR absorption of NiO nanoparticles is blue-shifted compared to that of the bulk form. The IR spectrum of NiO displays two

characteristic peaks appeared at 3445 and 1629 cm^{-1} [24]. However, there is some red or blue shift, which may be due to the small particle size of the prepared NiO. The infrared absorption spectrum changes of nano-materials was due to the quantum size role of the former factors were over the latter, the peak shifts from red to blue, and vice versa red shift to occur [25]. The absorption peak in the 2362 cm^{-1} was induced by the CO_2 in air adsorbed on the samples [26].

The optical characterization of the powder sample on transparent plaster has been preformed from spectral absorbance (αt) in the wavelength range extended from 200 to 2500 nm as shown in Fig. 7. The optical absorption data were analyzed using the following classical relation for near edge optical absorption in a semiconductor,

$$\alpha(h\upsilon) = \frac{K(h\upsilon - E_g^{opt})^{n/2}}{h\upsilon} \tag{3}$$

where k is a constant, E_g^{opt} is a semiconductor band gap and n a constant equal to 1* for direct transitions and 4 for indirect transition compounds [27]. The variation of $(\alpha t.\ h\nu)^2$ vs. $(h\nu)$ for the sample is shown the inset of Fig. 7. The nature of the graphs reveals that the optical absorption in this sample takes place through direct interband transitions. The extrapolation of the linear portion of the curve to zero absorption coefficient gives the value of optical band gap energy, E_g^{opt} = 3.81 eV. The energy gap value is in a good agreement obtained by Rifaya et al. for NiO, E_g^{opt} = 3.83 eV [28].

4- Conclusions

Fine NiO nanoparticles were prepared by a homogeneous precipitation method with an aqueous solution of nickel nitrate hexahydrate and citric acid. Thermo gravimetric (TGA) analysis and differential scanning calorimeter (DSC) were used to identify the calcination temperature for obtaining a high purity of NiO powder. The experiment results for both X-ray diffraction (XRD), scanning electron microscope (SEM) show that the NiO nanoparticles are cubic structure with spherical shape and well dispersed, the particle size distribution ranging from 7 to 28 nm with the average particle size is about 15.5 nm. The infrared absorption band of NiO nanoparticles shows blue shifts compared with that of bulk NiO. The optical band gap energy value 3.81 eV has been determined from absorbance spectra in strong absorption region

Acknowledgment

The author is grateful to El Minia University Faculty of Science Physics Department for financial support. I thank Dr. E. R. Shaaban, Al-Azhar University Faculty of Science Physics Department Assuit branch for measuring the DSC curve. Special thankfulness for Prof. Dr. MG.S.Ali El Minia university Faculty of Science Physics department for his valuable discussion during preparing the paper.

References

[1] D.Y. Goswami, S. Vijayaraghavan, S. Lu, G. Tamm (2004) Sol. Energy, 76: 33.

[2] M. Conte, P.P. Prosini, S. Passerini (2004) Mater. Sci. Eng. B 108: 2.

[3] SUN Quan, SHAO Zhong- cai, GAO Jing- long, J. Non- Ferrous Mining and Metallurgy 22 (2006) 40.

[4] I. Hotovy, J. Huran, P. Sicilano, et al. J. Sensors and Actuators B, 103(2004) 300.

[5] R. Service. Science, 313 (2006) 902

[6] H. Lu, W. Dai, M. Zheng, N. Li and J. Cao. J. Power Sources, 209 (2012) 243.

[7] I.S.Lee, N. Lee, J. Park, B.H. Kim, Y.W. Yi, T. T.K. Kim, I.H. Lee , S.R. Paik, T. Hyeon (2006) J Am Chem Soc 128: 10658**.**

[8] Yunpu Zhai, Yuqian Dou, Dongyuan Zhao, Pasquale F. Fulvio, Richard T. Mayes and Dai. Sheng Adv. Mater., 23 (2011) 4828

[9] K. De Wael, A. Verstraete, S. Van Vlierberghe, W. Dejonghe, P. Dubruel and A. Adriaens. Int. J. Electrochem. Sci., 6 (2011) 1810

[10] M.A. Khadar, V. Biju, A. Inoue (2003) Mater Res Bull 38: 1341.

[11] P. Poizot, S. Laruelle, S. Grugeon, L. Dupont, J–M Tarascon (2000) Nature 407: 496.

[12] H. Gleiter, Acta Mater. 48(2000) 1.

[13] C. Feldman, H.O. Jungk (2001) Angew. Chem. Int. Ed. 40: 359.

[14] V. Biji, M.A. Khadar (2001) Mater. Sci. Eng. A 304: 814.

[15] J.E. Rodriguez-Paez, A.C. Caballero, M. Villeggas, C. Moure, P. Duran, J.F. Fernandez (2001) J Eur Ceramic Soc.21: 925.

[16] M.I. Alymov, O.N. Leontieva (1995) NanoStruct Mater. 6: 393.

[17] F. Porta, S. Recchia, C. Bianchi, F. Confalonieri, G. Scari (1999) Colliods Surf (A): Physicochem Eng Aspects 155: 395.

[18] P.L. Llewellyn, V. Chevrot, J. Ragai, O. Cerclier, J. Estienne, F. Rouquerol (1997) Solid State Ionics,101–103: 1293

[19] M. Alagar, T. Theivasanthi, Raja A Kubera (1012) J. of App. Sci, 12: 398.

[20] M. El-Hagary, M. Emam-Ismail, E.R. Shaaban, A. Al-Rashidi, S. Althoyaib, Materials Chemistry and Physics 132 (2012) 581.

[21] T. Theivasanthi, M. Alagar, Nano Biomed (2011) Eng., 3: 163.

[22] http://imagej.nih.gov/ij.

[23] E. R. Shaaban, Appl Phys A 115 (2014) 919.

[24] L. Barrientos, *S. Rodriguez-Llamazares, J. Merchani, P. Jarai, N. Yutronic, V. Lavayen*, J. Chil. Chem. Soc., 54 (2009) 4.

[25] WANG Yan- ping, ZH U Jun-wu, ZHANG Li li, et al. J . Spectro scopy and Spectral Analysis 26 (2006) 690.

[26] WU Li li, WU You shi, WEI H ui ying , et al. Materials Letters, 58 (2004) 2700.

[27] T.S. Moss (1961) Optical Properties of Semiconductors, Butterworths, London 34.

[28] M. Nowsath Rifaya, T. Theivasanthi*, M. Alagar Nanoscience and Nanotechnology 2 (2012) 134.

Figure captions

Fig.1: TGA and DSC curves of the precursor.

Fig.2: DSC traces for Ni/NiO and NiO overlapped phases at heating rate 10 ^{o}K/min.

Fig.3: X-ray diffraction spectra of precursor at different annealing temperatures.

Fig.4: SEM image of NiO nanoparticles.

Fig.5: Particle size distribution of NiO nanoparticles

Fig.6: IR absorbance spectra of NiO nanoparticles.

Fig.7: UV-Vis-NIR absorbance spectrum of Ni/NiO nanoparticles.

The inset shows variation of $(\alpha t.\ h\nu)^2$ vs. $(h\nu)$ for NiO nanoparticles.

Table 1: Full width at half maximum and crystallize size of Ni/NiO and NiO nanoparticle Phases with different annealing temperature.

Pos. [2θ°]	d-spacing [Å]	FWHM	CrystalliteSize (nm)	Related peak
T = 335 °C				
37.009	2.4291	0.4133	21.162	NiO
43.165	2.0959	0.3822	23.337	NiO
44.241	2.0474	0.4133	21.663	Ni
51.602	1.7713	0.4326	21.296	Ni
62.672	1.4824	0.4810	20.188	NiO
T = 350 °C				
37.438	2.4022	0.4452	19.671	NiO
43.001	2.1034	0.4372	20. 390	NiO
44.212	2.0486	0.4991	17.937	Ni
62.607	1.4826	0.5122	18.952	NiO
T = 365 °C				
37.176	2.4186	0.5904	14.822	NiO
43.244	2.0922	0.5532	16.128	NiO
62.451	1.4859	0.7200	13.471	NiO

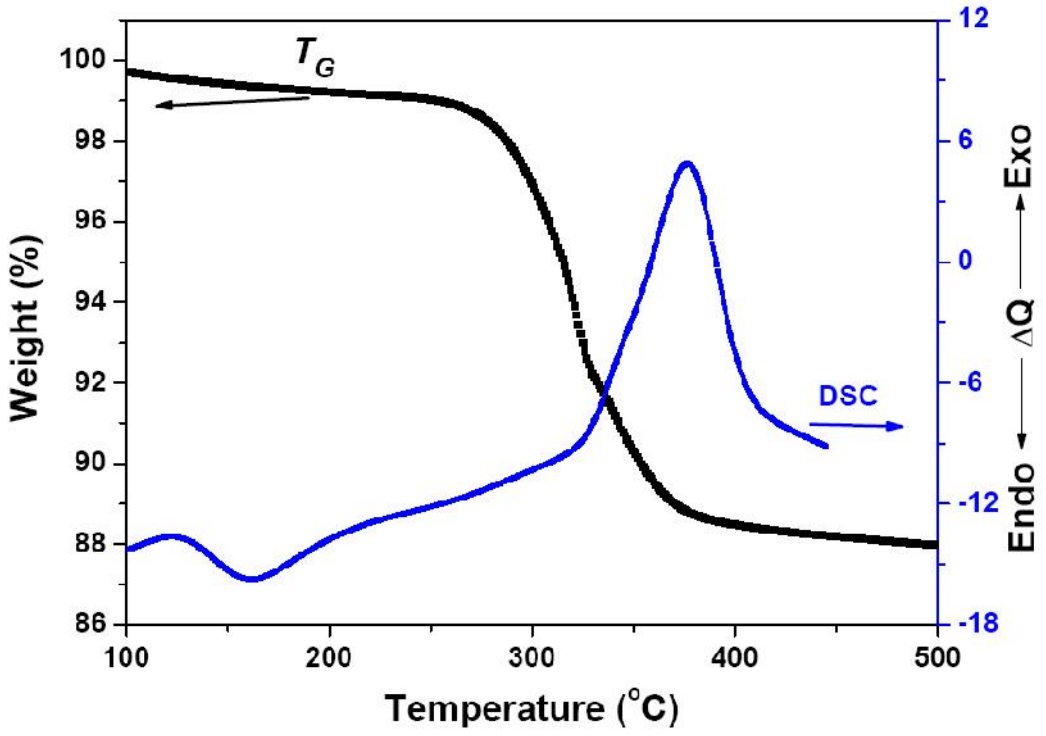
T_G
DSC
Weight (%)
Temperature (°C)
ΔQ
Exo
Endo
100
98
96
94
92
90
88
86
12
6
0
-6
-12
-18
100
200
300
400
500

Fig. 1

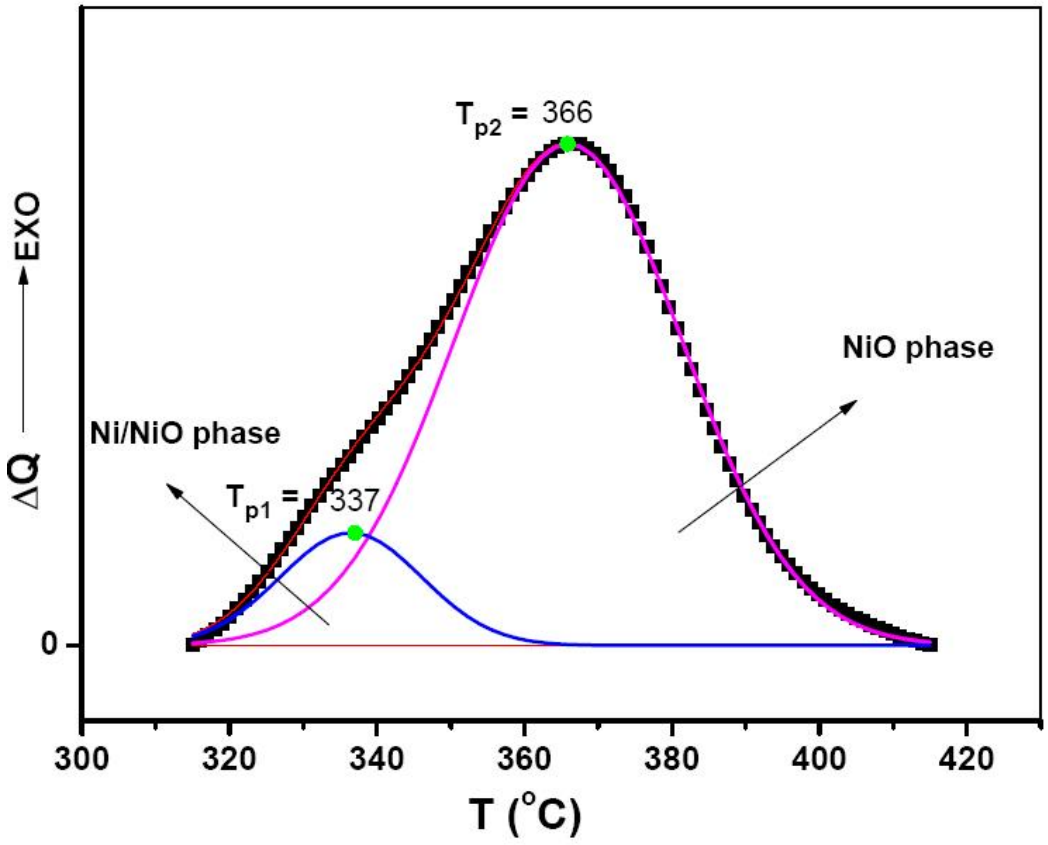
T_{p2} = 366
EXO
ΔQ
NiO phase
Ni/NiO phase
T_{p1} = 337
0
300
320
340
360
380
400
420
T (°C)

Fig. 2

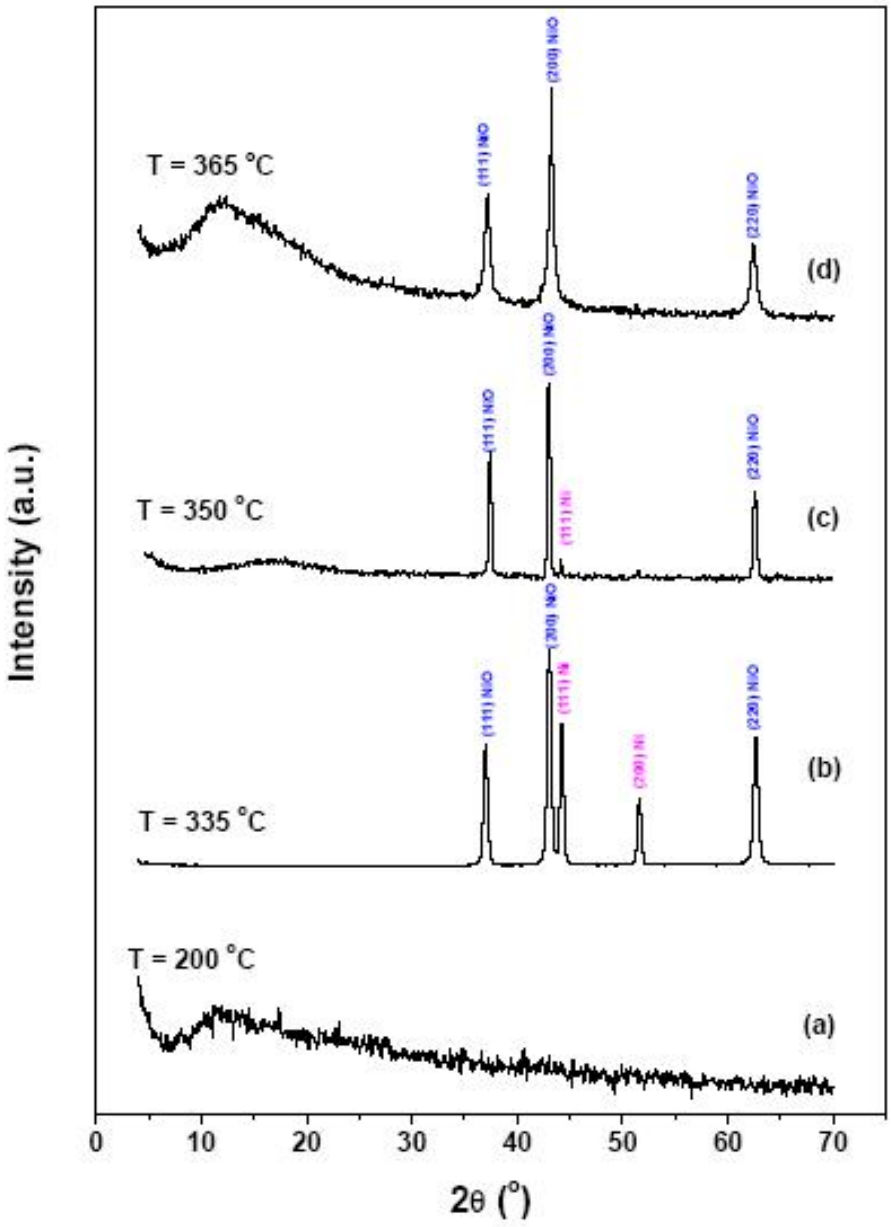
Intensity (a.u.)
T = 365 °C
T = 350 °C
T = 335 °C
T = 200 °C
(a)
(b)
(c)
(d)
(111) NiO
(200) NiO
(220) NiO
(111) Ni
(200) Ni
0
10
20
30
40
50
60
70
2θ (°)

Fig. 3

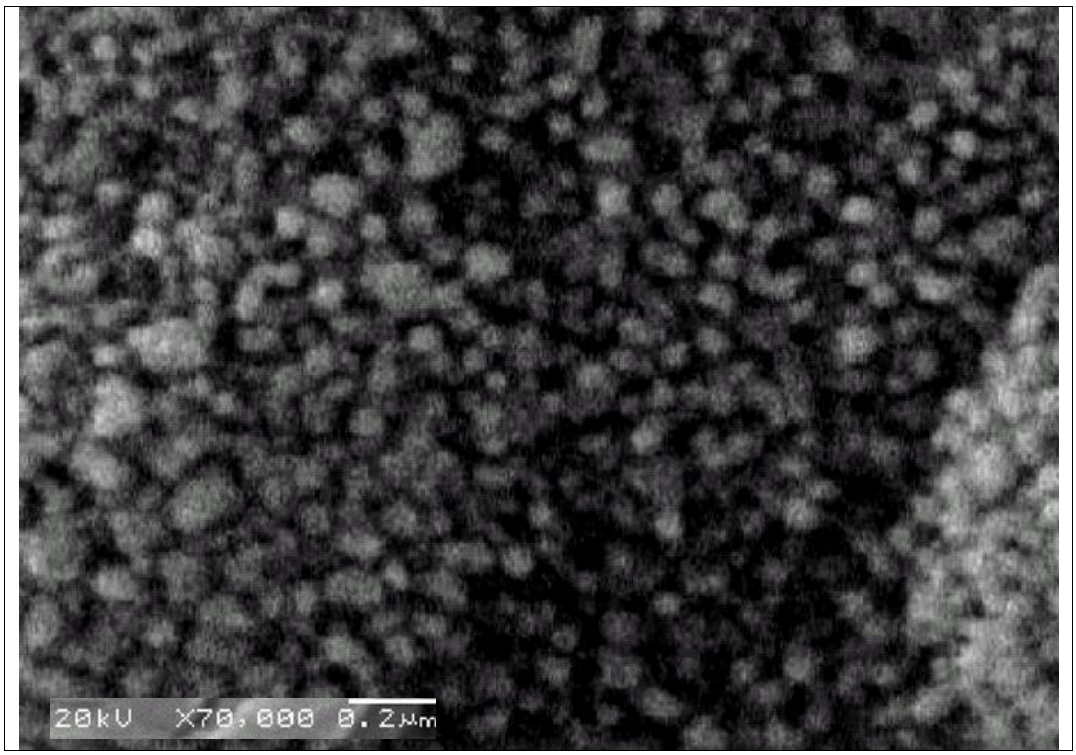

Fig. 4

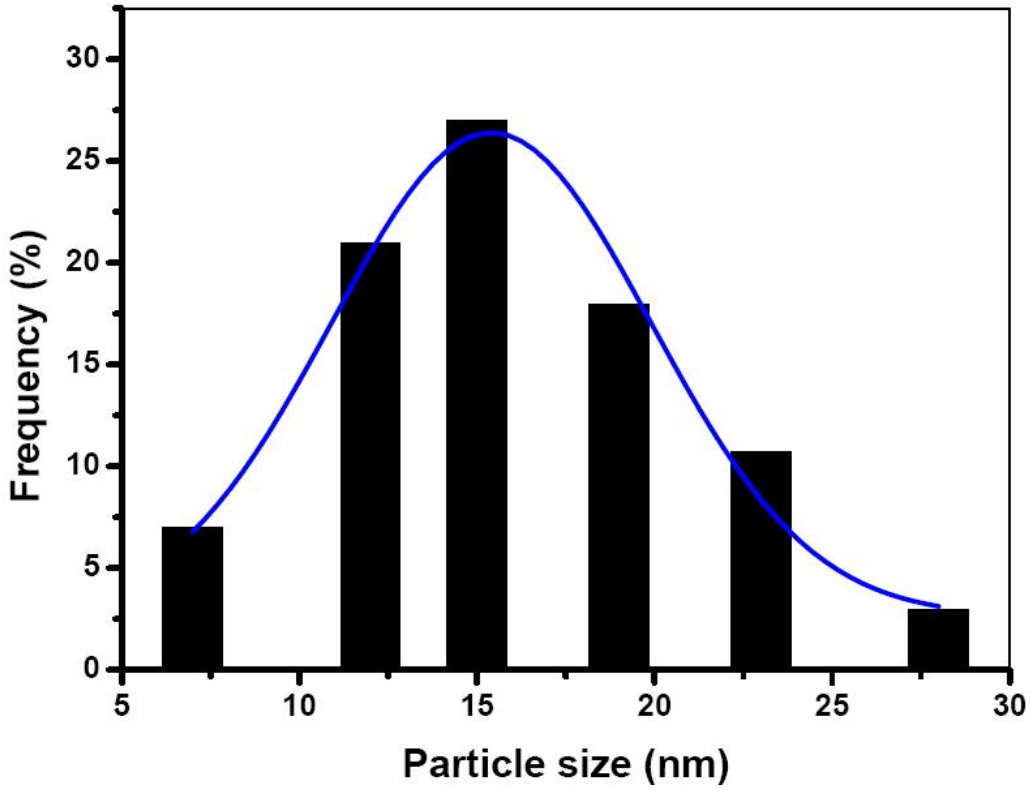

Fig. 5

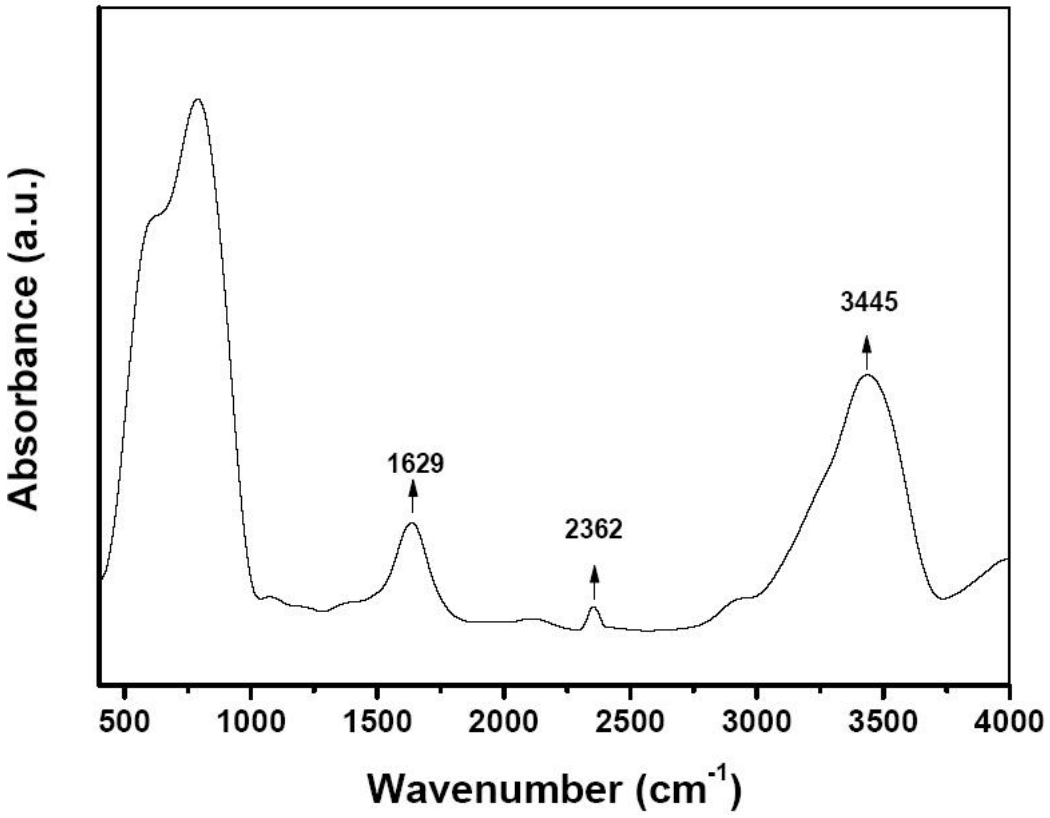
Absorbance (a.u.)
3445
1629
2362
500
1000
1500
2000
2500
3000
3500
4000
Wavenumber (cm-1)

Fig. 6

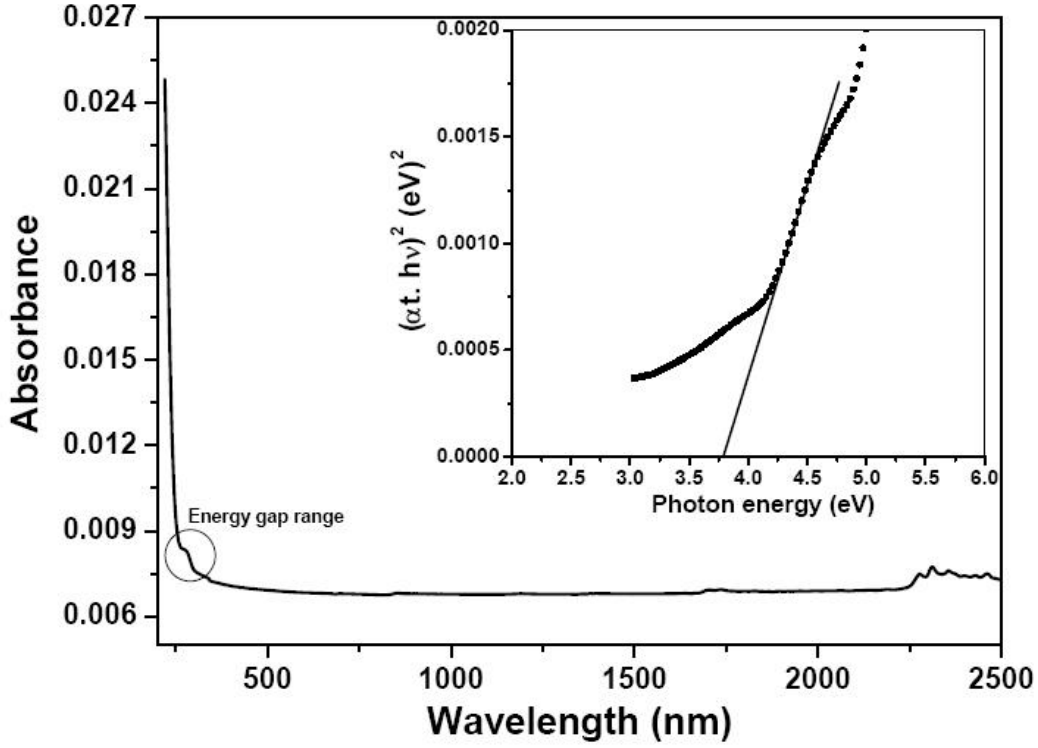
Absorbance
0.027
0.024
0.021
0.018
0.015
0.012
0.009
0.006
Energy gap range
500
1000
1500
2000
2500
Wavelength (nm)
$(\alpha t. h\nu)^2$ (eV)^2
0.0020
0.0015
0.0010
0.0005
0.0000
2.0
2.5
3.0
3.5
4.0
4.5
5.0
5.5
6.0
Photon energy (eV)

Fig. 7